LOCA Integral Test Results for High-Burnup BWR Fuel

Yong Yan, Michael C. Billone, Tatiana A. Burtseva, and Hee M. Chung
Argonne National Laboratory (ANL), Argonne, IL 60439

Abstract

Results from loss-of-coolant-accident (LOCA) integral tests are reported for high-burnup fuel-rod specimens from a boiling water reactor (BWR) at Limerick. These results are compared to baseline data for nonirradiated Zry-2 cladding specimens filled with zirconia pellets and exposed to the same tests. Four LOCA integral tests have been conducted with specimens from Limerick BWR fuel rods at burnup of 56 GWd/MTU. The ICL#1 test specimen was heated to bursting in argon and slowly cooled. The ICL#2 specimen was exposed to the LOCA test sequence with the exception of quench. The ICL#3 specimen achieved partial quench (800˚C to 470˚C) before failure of the quartz chamber that surrounded the specimen. The full LOCA sequence in ICL#4 calls for heating in steam at 5˚C/s to 1204˚C, holding for 5 minutes at 1204˚C (≤ 20% CP best-estimate ECR), slow cooling at 3˚C/s to 800˚C, and bottom-flooding to quench the cladding from 800 to 100˚C. Destructive examinations showed two-sided oxidation in the ballooned-and-burst region of both high-burnup and nonirradiated specimens. For nonirradiated specimens, the hydrogen pickup was low in the burst region and very high at 70-90 mm above and below the burst mid-plane. For high-burnup-fuel cladding, the hydrogen peak was toward the burst mid-plane. In addition, the effects of hydrogen on diametral-compression post-quench ductility (PQD) have been investigated with prehydrided (300-to-800 wppm hydrogen), nonirradiated 15x15 Zry-4 cladding rings after oxidation at 1204˚C and quench. The baseline data from prehydrided cladding are being used to plan the LOCA test times for specimens from a pressurized water reactor (PWR) such that the embrittlement equivalent cladding reacted (ECR) can be determined effectively in the ballooned and non-ballooned regions.

Introduction

The LOCA licensing criteria (10 CFR 50.46) limit peak cladding temperature to 2200°F (1204°C) and maximum oxidation (expressed as equivalent cladding reacted, ECR) to 17% to ensure cladding ductility during quenching from the emergency core cooling system and during possible post-LOCA events (e.g., seismic). In formulating these criteria, it was assumed that knowledge of the detailed loading modes and magnitudes experienced by the cladding, beyond the thermal stresses induced by rapid cooling, are not well defined. Cladding that retains some plastic ductility has more margin for surviving quench and post-quench loads without fragmenting compared with brittle cladding. Based on Appendix K of this regulation, the Baker-Just (BJ) correlation is to be used to calculate the metal-water (i.e., steam) reaction. Regulatory Guide 1.157 (1989) allows the use of a best-estimate correlation, such as the Cathcart-Pawel (CP) model, to calculate the oxidation rate in steam for T > 1900˚F (1038˚C). At 1204˚C, the ratio of the BJ-to-CP prediction is ≈1.3. To compensate for the possible effects of high burnup operation (e.g., hydrogen pickup), NRC Information Notice 98-29 (1998) defines total oxidation to include in-reactor corrosion (ECR_{ss}), as well as transient steam oxidation (ECR_t).

The LOCA integral tests at ANL, using high burnup fuel-rod segments from boiling and pressurized water reactors, are designed to address the adequacy of the embrittlement criteria, of the correlations (CP vs. BJ) used to calculate oxidation, and of the decrease in allowable transient oxidation ($ECR_t \leq 17\% - ECR_{ss}$) to compensate for the embrittling effects of hydrogen. In addition to this confirmatory aspect of the research, the fundamental behavior of high-burnup fuel and cladding, exposed to a LOCA transient, is investigated and characterized.

The LOCA-relevant research at Argonne National Laboratory (ANL) includes high-temperature steam oxidation studies of cladding [1], LOCA integral testing of fueled segments [2], post-quench ductility testing of LOCA integral specimens, and post-quench ductility testing of nonirradiated zirconium-based cladding alloys [3]. Four LOCA integral tests with high-burnup BWR samples (from Limerick fuel rods at 56 GWd/MTU) have been completed. The ICL#1 test specimen was heated to bursting in argon and slowly cooled. The ICL#2 specimen was exposed to the LOCA test sequence with the exception of quench. The ICL#3 specimen achieved partial quench (800˚C to 470˚C) before failure of the quartz chamber that surrounded the specimen. A full LOCA sequence in ICL#4 was completed in March 2004.

This paper presents the results of the post-test examinations of the ICL#1-4 samples: fuel morphology; cladding inner- and outer-surface oxidation within the ballooned region; post-test gamma scanning; fractography; and hydrogen pickup in the neck and ballooned regions. After completion of the high-burnup BWR test matrix, high-burnup PWR rods (from the H. B. Robinson reactor) will be subjected to the LOCA test sequence indicated in Fig. 1. Post-quench ductility (PQD) baseline data with prehydrided 15x15 Zry-4 cladding are also presented for the planning of the H.B. Robinson LOCA integral tests.

Experimental Procedure

LOCA integral tests consist of rapidly heating (5 °C/s) a 300-mm-long fuel segment under internal pressure in a steam environment, holding it at 1200°C for ≤5 minutes, cooling it (3 °C/s) to 800°C, and then quenching it with room-temperature water. A schematic illustration of the LOCA sequence is given in Fig. 1. The LOCA integral apparatus, as shown schematically in Fig. 2, contains the following features: radiant furnace, argon purge system, high-pressure system to internally pressurize the 300-mm-long test sample, steam supply system, and quench system.

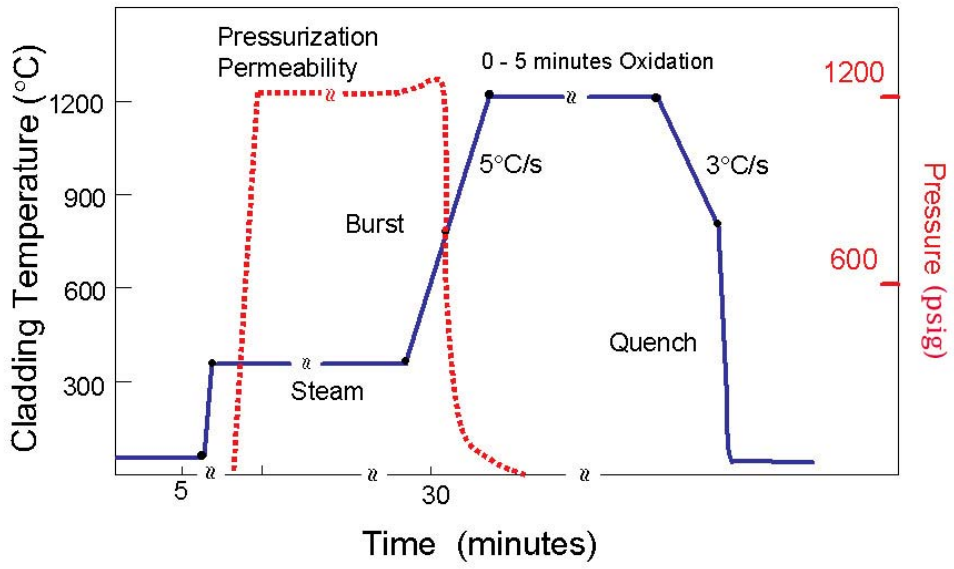

Fig. 1. Temperature and pressure histories for full LOCA integral test sequence, including quench from 800˚C to 100˚C.

A series of out-of-cell LOCA integral tests was conducted with unirradiated Zry-2 cladding at 1204°C in steam. The out-of-cell LOCA samples are used to benchmark the testing methods and to obtain data for post-quench ductility, as well as properties data for weight gain, oxide-alpha-beta layer thicknesses, and hydrogen and oxygen distributions. This data set serves as a baseline for in-cell LOCA tests with high-burnup-fuel samples.

Results for the OCL#11 (an out-of cell LOCA test with unirradiated 9x9 Zr-2 for 5 minutes at 1204˚C), companion test to ICL#2, are briefly discussed here. The concentrations of oxygen and hydrogen were measured by the LECO method after the OCL#11 test. These concentrations are referenced to the weight of the oxidized samples. The data need to be converted to concentrations referenced to the pre-oxidized sample weight in order to determine pickup values during the transient. The algorithms for calculating oxygen and hydrogen pickup from the LECO data were given in our previous work [3]. In addition, quantitative metallography (see Fig. 3), along with the CP models for interface oxygen concentrations and diffusion within the oxide, alpha, and beta layers, was used to determine the weight gain per unit surface area and the corresponding ECR.

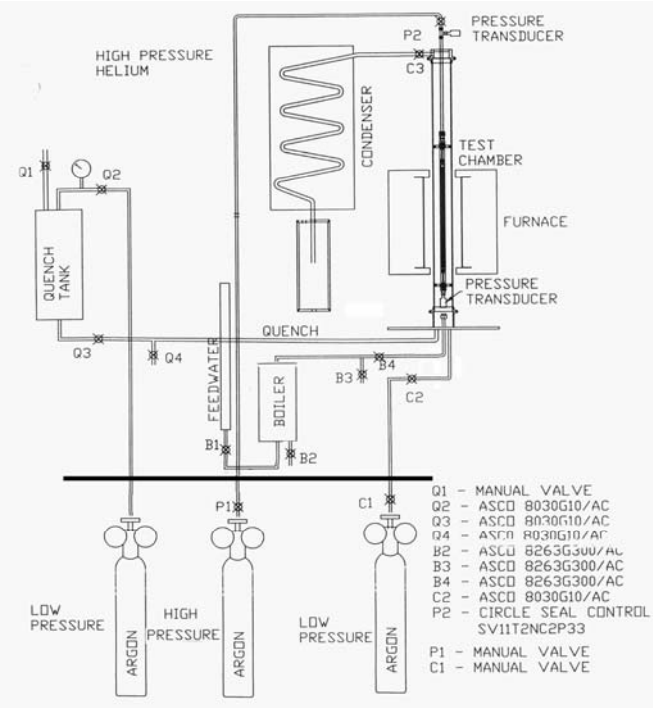

Fig. 2. Schematic illustration of LOCA system.

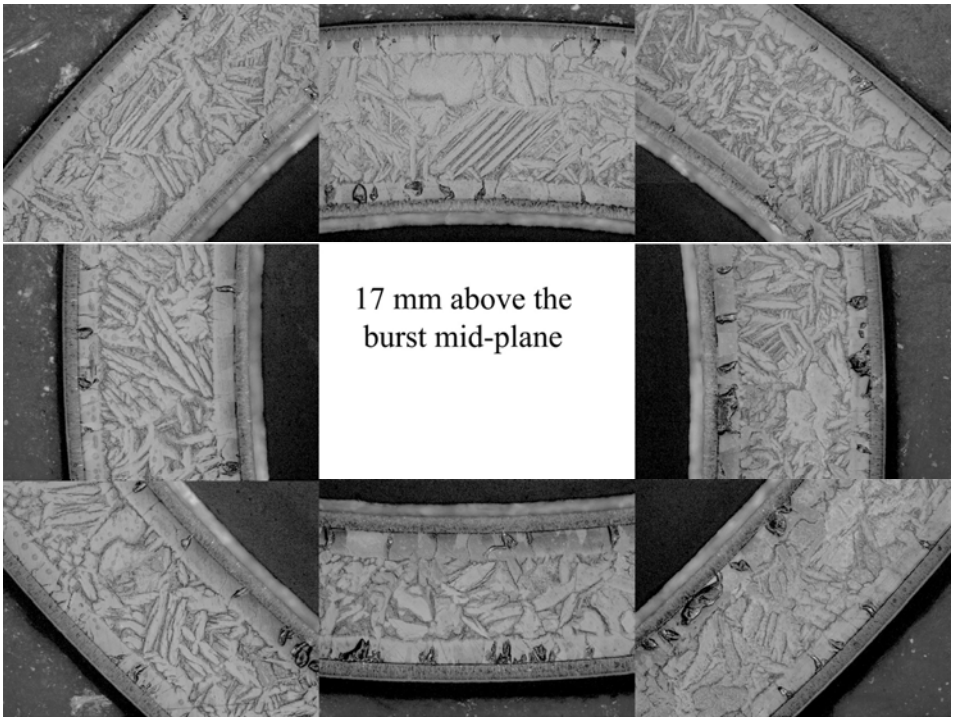

Fig. 3. Cladding metallographic results for OCL#11 specimen.

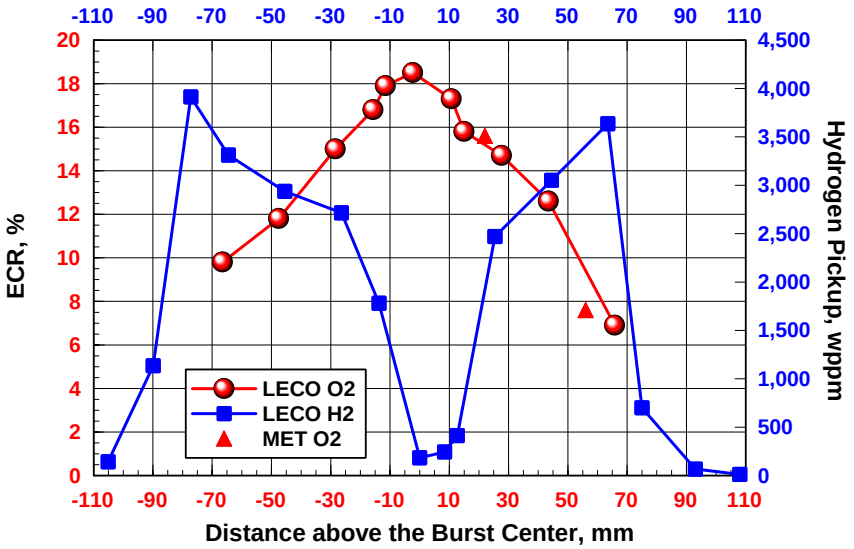

Fig. 4. Axial distributions of hydrogen pickup and ECR for out-of-cell test OCL#11 with nonirradiated Zry-2 cladding. The average values do not give information regarding the local concentrations of oxygen and hydrogen across the wall of the cladding. Oxygen concentrations in the oxide and alpha layers are much higher than the average value, while hydrogen concentration in the prior-beta layer is much higher than the average concentration.

The axial distributions of ECR and hydrogen pickup of the OCL#11 sample are shown in Fig. 4. As expected, the oxygen pickup and ECR peak at the center of the burst region where the cladding is thinnest and the oxidation is fully two-sided. The ECR decreases away from the burst center as the cladding wall thickness increases and the degree of inner-surface oxidation decreases. Also, as expected, the hydrogen pickup, due to secondary hydriding, peaks near the balloon neck regions. The magnitude of these hydrogen peaks, however, is larger than previously reported [4] and may depend on ballooning strain profile, burst opening, diameter of pellets (zirconia) inside the cladding, heating method (internal vs. external vs. direct-electrical), and cladding type (lined Zry-2 vs. Zry-4). As these hydrogen peaks, as well as the hydrogen within the balloon region, are potentially embrittling, it is important to determine the magnitude of such effects for high-burnup cladding. Additional nondestructive examination results and some destructive results for the OCL#11 sample were reported in Ref. 3.

LOCA In-cell Integral Test Results

Limerick Rod J4 was selected for the in-cell LOCA tests ICL#3 and ICL#4. Based on our gamma scan data (see Fig. 5), there appear to be no unusual features in the pre-test specimens. Figure 6 shows the temperature and pressure histories for the ICL#4 test at an average hold temperature of ≈1204˚C for 5 minutes in steam. Two thermocouples (180° apart) were strapped at 2-inches above the mid-plane, and the temperature difference between them was less than 14°C.

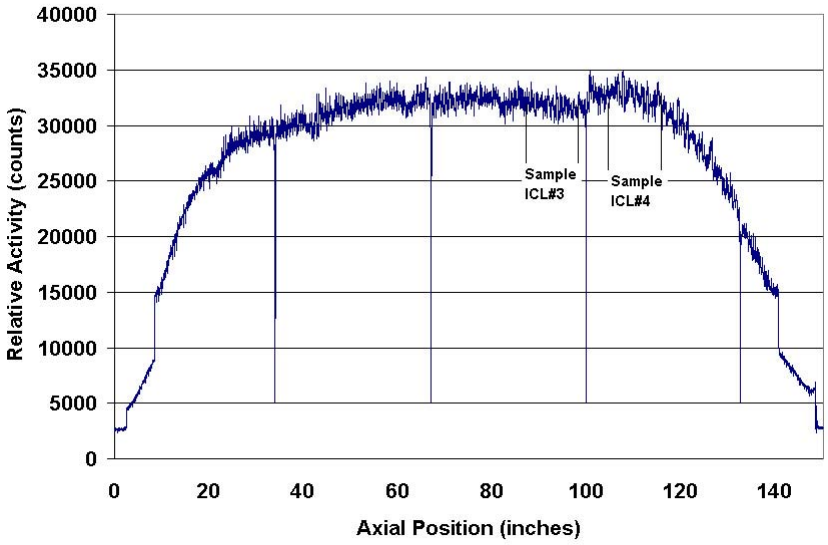

Fig.5. Gamma scan profile of Limerick fuel rod J4.

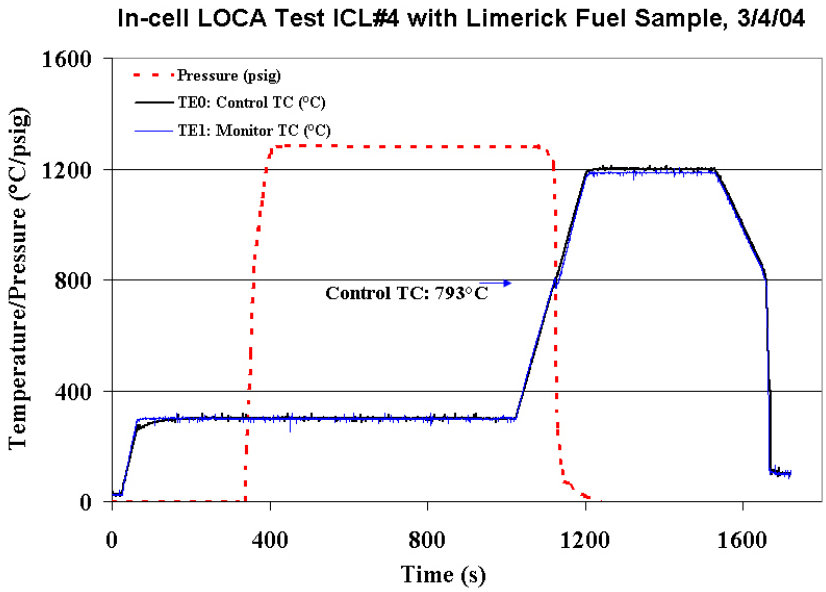

Fig.6. Temperature and pressure histories of in-cell LOCA test ICL#4.

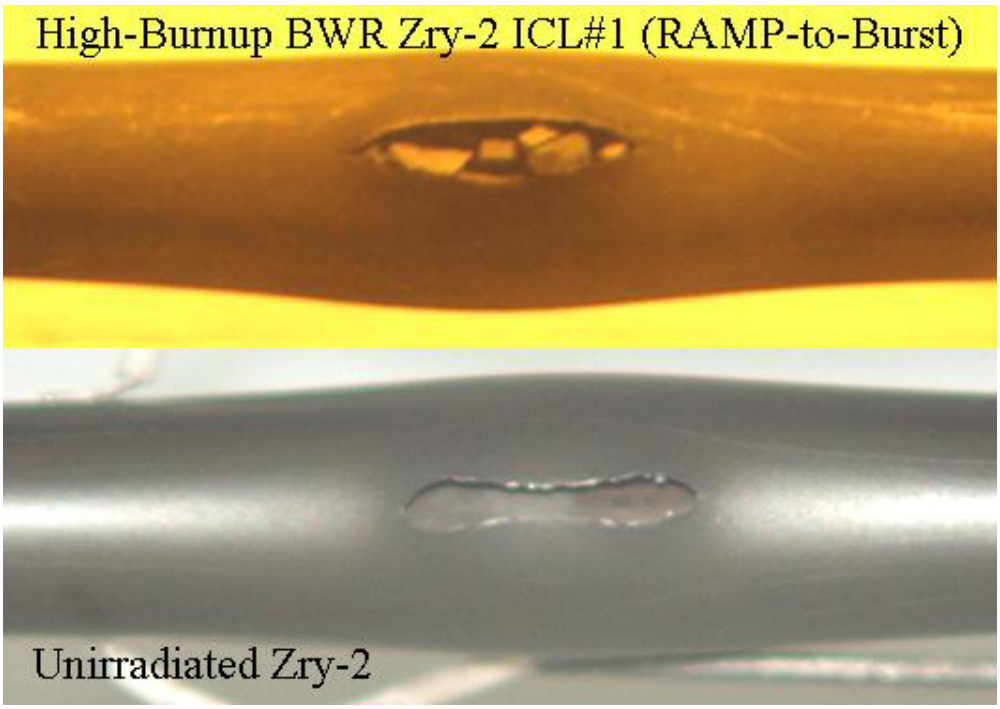

Fig. 7. High magnification micrographs of the burst opening for ramp-to-burst tests.

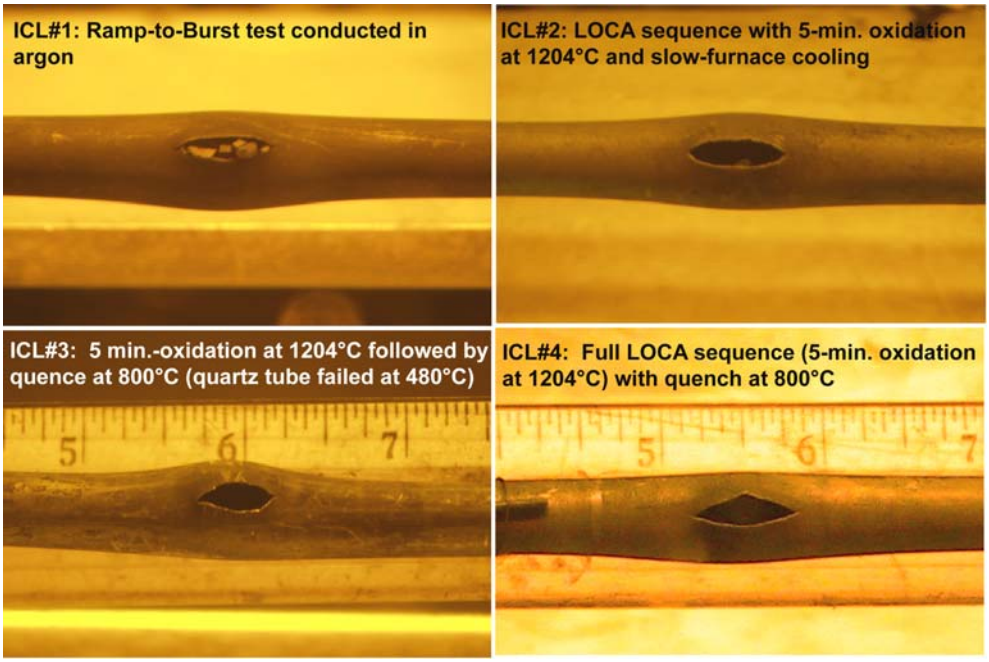

Fig. 8. Micrographs showing the balloon and burst regions for ICL#1 – #4 specimens.

Nondestructive Characterizations

Nondestructive characterizations for the ICL#1 - #4 samples were completed shortly after the tests. The results are summarized in Table 1. Unlike the dog-bone burst shape of the unirradiated OCL#11 sample (see Fig. 7), an oval burst shape was observed for all LOCA in-cell samples (see Fig. 8). The burst temperatures for the LOCA in-cell tests range from 730 to 790°C, and their burst lengths are in the range of 11-15 mm. In addition, the balloon lengths (defined by OD strains ≈2%) of the LOCA in-cell samples are shorter than that of the LOCA out-of-cell sample. No significant difference was found for the maximum OD strain between the unirradiated samples and the high-burnup samples.

Axial Locations of Specimens for Destructive Evaluation

Figure 9 shows the axial locations at which sample ICL#3 was broken (locations A, B, and C) during the sample handling, before the sectioning was performed at location D. Metallographic examinations were conducted at location B, and scanning electron microscopy (SEM) examinations were conducted at locations A and C. The hydrogen and oxygen analysis samples were further sectioned from the specimens A-B and C-D.

Table 1. Summary of in-cell LOCA integral tests (ICL) with high-burnup fueled cladding specimens from Limerick BWR. Also shown are the results of out-of-cell test OCL#11 with non-irradiated Zry-2 cladding.

Parameter	ICL#1	ICL#2	ICL#3	ICL#4	OCL#11
Hold Time, minutes	0	5	5	5	5
Max. Pressure, MPa	8.96	8.87	9.0	8.86	8.61
Burst Pressure, MPa	≤8.61	≤8.01	8.6	8.0	≤7.93
Burst Temperature, °C	≈755	≈750	≈730	≈790	≈ 750
Burst Shape	Oval	Oval	Oval	Oval	Dog Bone
Burst Length, mm	13	14	11	15	11
Max. Burst Width, mm	3	3.5	4.6	5.1	1
Length of Balloon, mm	≈ 70	≈ 90	≈ 100	≈ 80	≈ 140
$(\Delta D/D_o)$max, %	38±9	39±10	43±9	36±9	43±10
Max. Calculated ECR, %	0	≈20	≈21	≈20	≈21
Max. ΔH, wppm	…	> 220	≥ 2900	TBD	3900

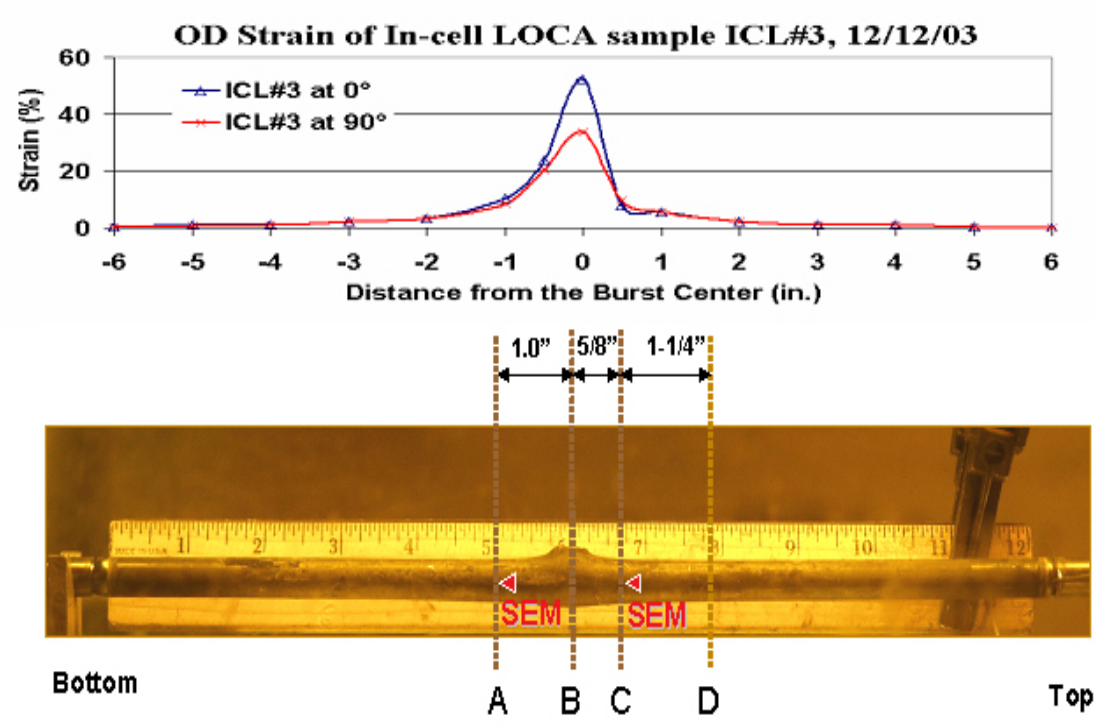

Fig. 9 Post-test characterization for ICL#3 sample. The ICL#3 sample was broken at axial positions A, B, and C during the sample handling.

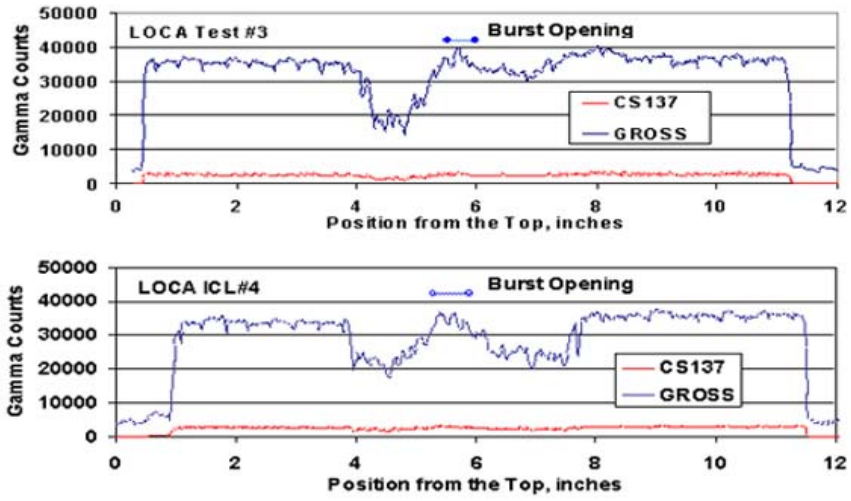

Fig. 10. Gamma scan profiles for ICL#3 and ICL#4 specimens.

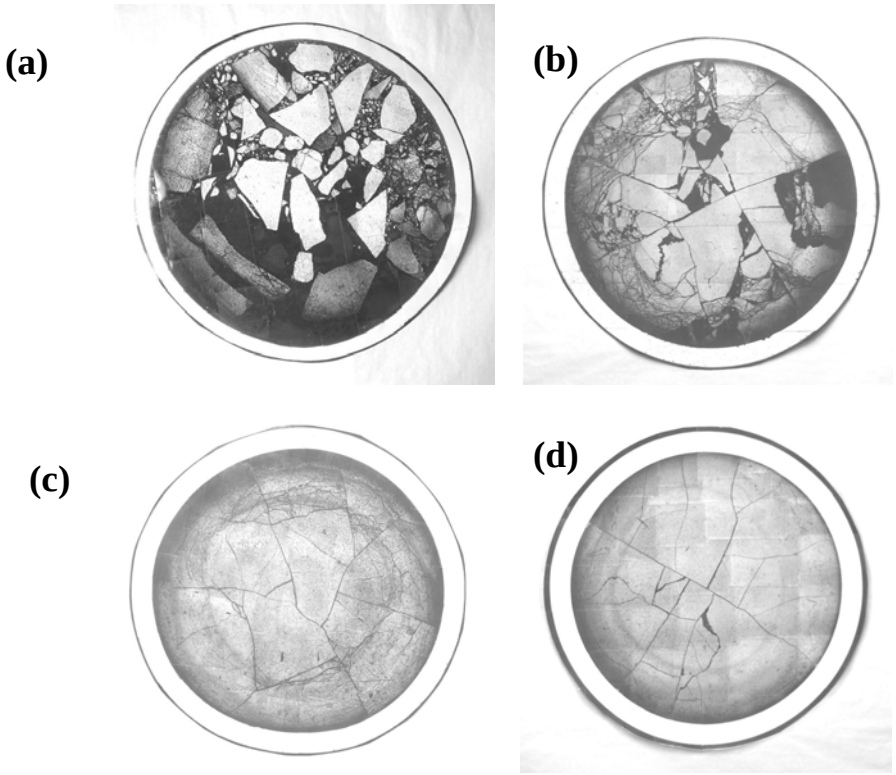

Fig. 11. Low-magnification images of the post-LOCA test ICL#2 fuel samples at ≈12 mm above the burst center (a); ≈50 mm above the burst center (b); ≈130 mm below the burst center (c); and the Limerick fuel prior to LOCA testing (180 mm from the LOCA sample) (d). Cladding diametral strains are 2-4% for the Fig. 11b cross section and 15-25% for the Fig. 11a cross-section.

Fuel Relocation

There is considerable interest in the behavior of high-burnup fuel during a LOCA transient. Prior to the transient, the fuel is tightly bonded to the cladding. During ballooning, the cladding pulls away from the fuel. This allows space for fuel particles (macro-cracked, micro-cracked, and very small particles from the rim layer) to fall into the balloon region. If such movement were to result in a local increase in fuel per unit length, then the higher decay heat per unit length would increase cladding oxidation temperature and maximum ECR in the burst region. Also, if the fuel-cladding bond material moves with the cladding, such a layer could slow down the initial steam oxidation rate and could protect the cladding from the large hydrogen absorption observed in tests with bare-wall, nonirradiated cladding (see Fig. 4). As methods that could be used to freeze the fuel particles in place (e.g., epoxy) conflict with cladding characterization, the ANL program is more focused on the details of cladding oxidation, hydriding, and ductility than on fuel behavior. This focus was certainly the case for the ICL#2 sample, as no attempt was made to prevent fuel fallout during handling. For the ICL#3 and ICL#4 samples, the burst areas were taped following the test to minimize fuel fallout and the samples were gamma-scanned – prior to other nondestructive characterizations – to determine the axial distribution of fuel in and beyond the balloon region. Figure 10 shows the gamma scan profiles for the ICL#3 and ICL#4 specimens. For the axial locations with little-to-no permanent strain, gamma counts received from the fuel most likely represent the condition of the fuel at the end of the LOCA test. For the ICL#3 and ICL#4 balloon regions, some redistribution of fuel particles likely took place between the end of the LOCA test and the gamma scan due to the sample handling and transfer.

Figure 11 shows low-magnification images of the fuel structure of the ICL#2 sample at axial locations: (a) ≈12 mm above the burst center, (b) ≈50 mm above the burst, and (c) ≈130 mm below the burst center (45 mm above the bottom end-cap). Also shown is (d) the fuel structure of the as-received Limerick fuel. The structures of Figs. 11c and d are similar, except that the post-LOCA fuel shows a ring of circumferential tearing about mid-radius. This tearing may have occurred as the cladding tried to move a small distance (0.1 mm) away from the fuel and/or because the fission-product gases affected the fuel (see dark ring near mid-radius for the pre-LOCA fuel in Fig. 11d). At ≈50 mm above the burst, the circumferential tearing is enhanced as compared to the ≈130-mm location, most likely due to the larger cladding strain. Some fuel fallout may have occurred during cutting, although this region of the fuel column was embedded in a soft epoxy prior to cutting. Smaller fuel particles are also observed. In Fig.

11a, a wide range of fuel particles is observed, although these particles and fuel chunks are not co-planar. The particles and chunks are held in place by soft epoxy. Because this photograph was taken after extensive handling of the sample, resulting in axial redistribution of particles and fuel fallout through the burst opening, it does not represent the fuel condition near the burst center during the LOCA test or after the quench. The most that one can glean from such a picture is that the wide range of fuel-particle sizes would allow some fuel to fall from <50 mm above the burst center to the burst region.

Cladding Metallography

Low-magnification photographs were taken at 16 circumferential locations of the burst midplane of the ICL#3 sample and pieced together (see Fig. 12a) to obtain an image of the metal (oxygen-stabilized alpha and prior-beta) thickness vs. circumferential location, as compared to the cladding structure of the unirradiated material (see Fig. 12b). The inner and outer oxide layers are not visible in Fig. 12a. Also, the burst tips, which are very thin and heavily oxidized, are likely lost in the cutting process.

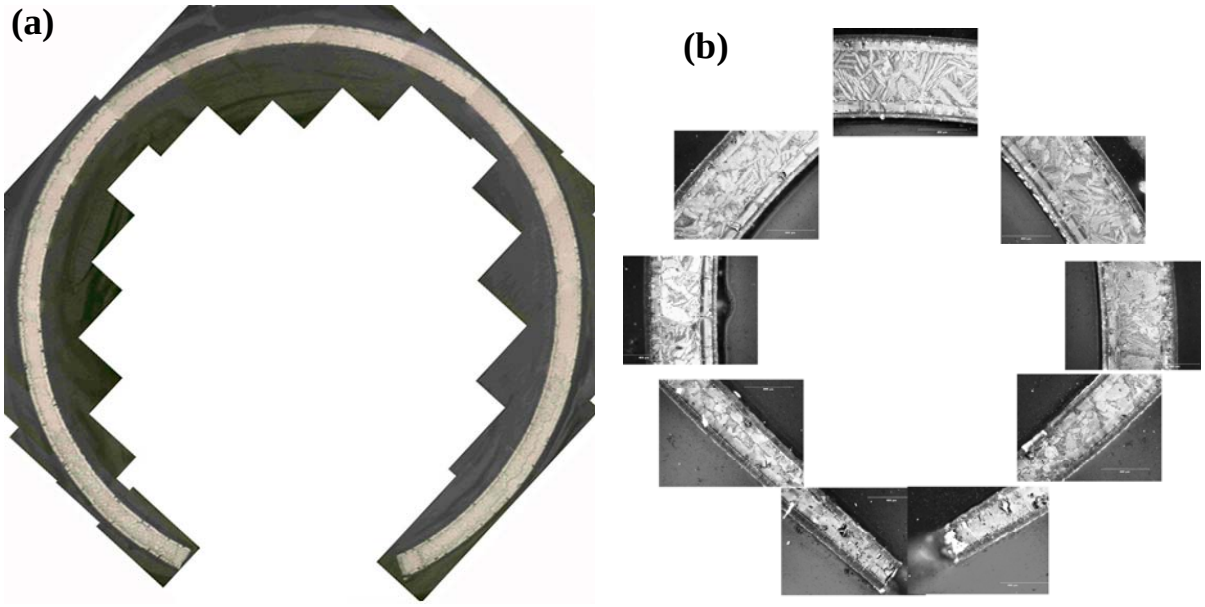

Fig. 12. Composites of the cladding cross section at the burst midplane of the in-cell LOCA sample ICL#3 (a) and the out-of-cell LOCA sample OCL#11 (b). The tips of samples were lost during the post-test sample handling.

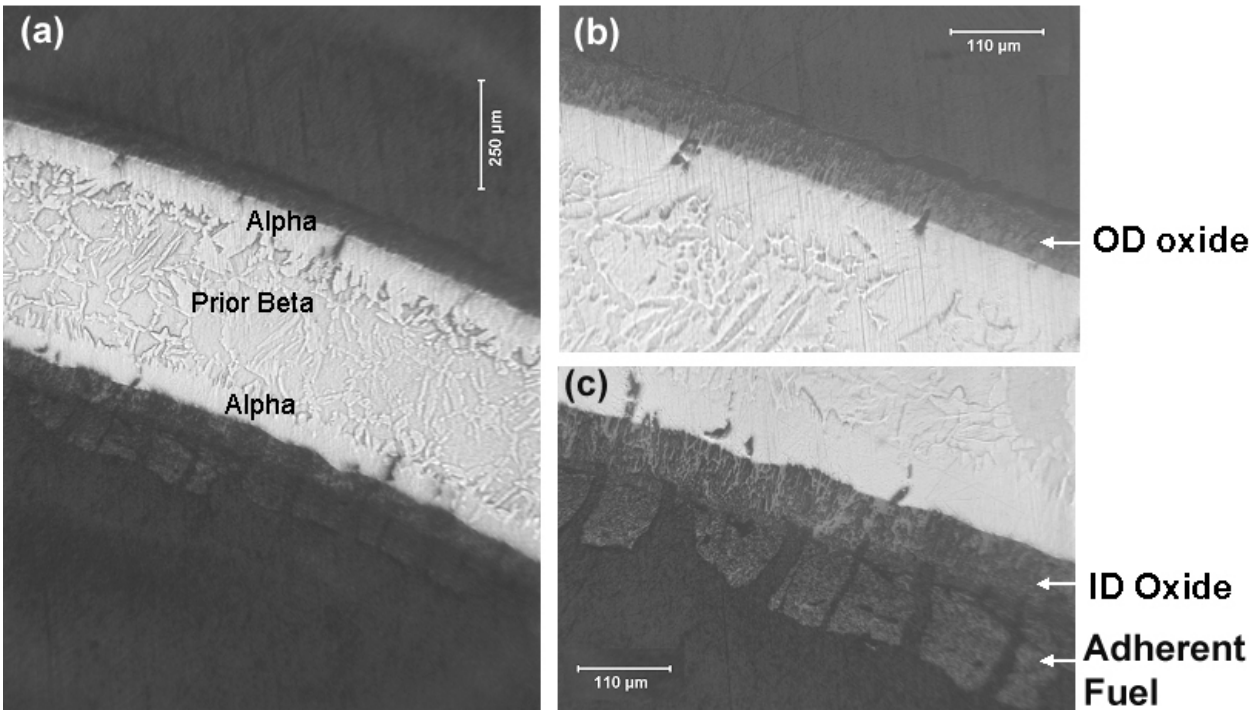

Fig. 13. Metallographic images of the ICL#3 specimen at the burst midplane. Micrograph (a) shows well-defined alpha layers that formed at 1200˚C and large prior-beta grains surrounded by oxygen-stabilized alpha layers formed during slow cooling to 800˚C; and micrographs(b) and (c) show good definition of the outer- and inner-surface oxide layers.

High-magnification micrographs were obtained of the inner and outer cladding regions away from the burst tips. These are shown in Figs. 13b (outer surface) and 13c (inner surface). The thickness of the outer-surface oxide layer is consistent with the CP-calculated oxide thickness and with the results from oxidation tests conducted on undeformed cladding samples [2]. The results demonstrate that the ≈10-µm-thick corrosion layer is not protective with regard to steam oxidation. The inner-surface oxide layer is wavy in appearance, which is likely due to the high hydrogen-to-steam ratio within the burst region. It is comparable in thickness to the outer-surface layer, which suggests that the fuel-cladding bond layer is also not protective with regard to steam oxidation. Alpha incursions into the prior-beta layer are observed at this location, just as they were observed in the oxidation tests. These most likely formed during the 3˚C/s cooling from 1200˚C to 800˚C. They represent regions with higher oxygen content than the remaining prior-beta material and lower oxygen content than the alpha layer that was formed at 1200˚C. Adherent fuel was observed on the inner surface of the ICL#3 burst region, as shown in Fig. 13c.

More detailed metallography was obtained for the ICL#2 specimen at the axial position 12 mm above the burst midplane. Double-sided oxidation is evident at this location, with the thickness of the inner-surface oxide layer greater than that of the outer-surface. Quantitative metallography was performed to determine the distribution of cladding thickness and outer-surface oxide-layer thickness (inner and outer) with respect to circumferential orientation. These results are compared to the baseline results obtained for the nonirradiated Zry-2 sample used in the OCL#11 test. To focus on the transient oxidation of the high-burnup LOCA sample (ICL#2), 10 μm was subtracted from the total outer-surface oxide-layer thickness to generate the transient oxidation data. For the OCL#11 sample, the weight gain and ECR at this location were determined to be 11.4 mg/cm^2 and 15.7%, respectively, while the prior-beta-layer thickness was measured to be 398 μm. The high-burnup sample differs somewhat in that there is more circumferential variation in the inner-surface oxide-layer thickness. The weight gain and ECR were determined to be 10.5 mg/cm^2 and 14.9%, respectively, while the prior-beta-layer thickness was measured to be 435 μm for the ICL#2 sample at this location. Although the axial locations with respect to the burst center are slightly different (18 mm above for OCL#11 and 12 mm above for ICL#2), the values for oxide-layer thickness, weight gain, ECR, and prior-beta-layer thickness are remarkably close. These results indicate that close to the burst region the steam oxidation of both nonirradiated and high-burnup Zry-2 samples is essentially the same. No significant high-burnup effects were observed.

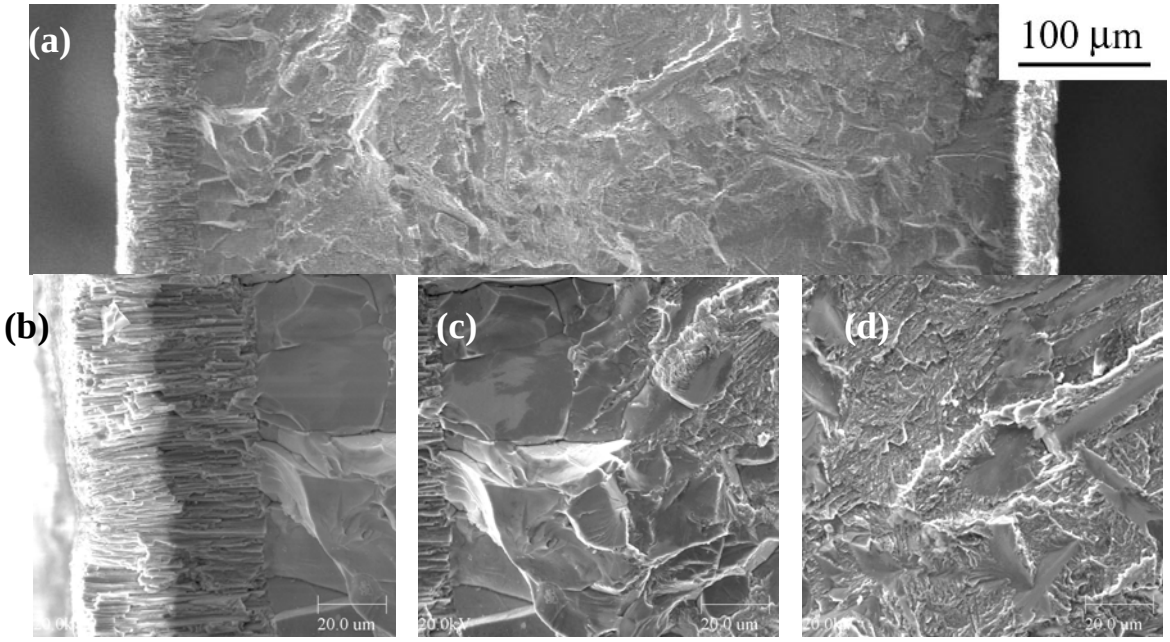

Fig. 14. Fractography of ICL#3 sample at the location of 20 mm above the burst midplane.

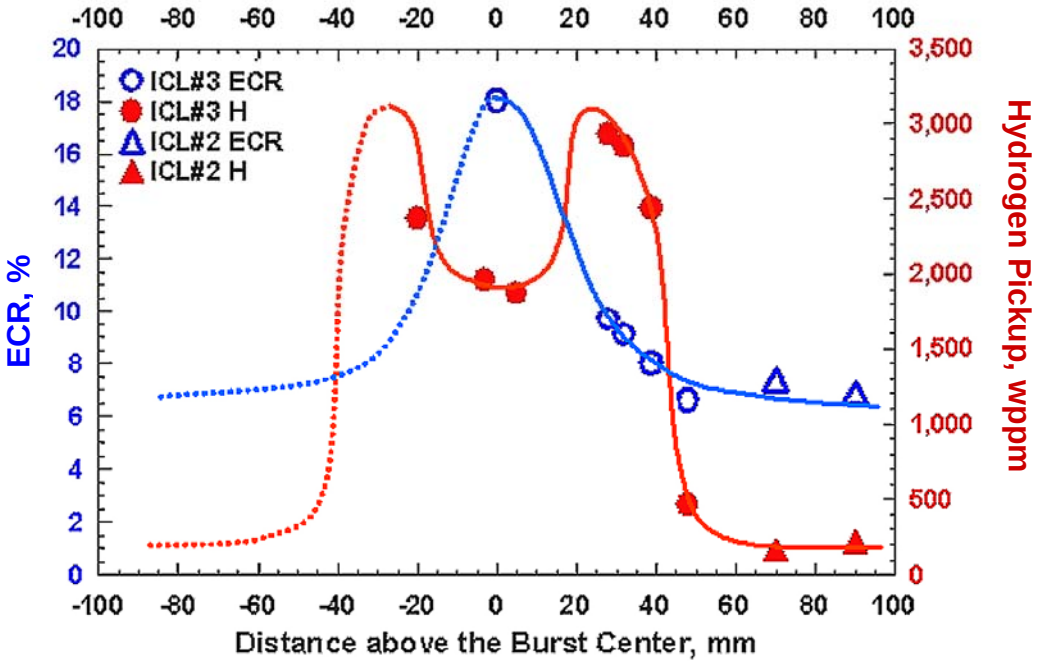

Fig. 15. Axial distributions of hydrogen and ECR for in-cell LOCA tests ICL#2 and ICL#3 with high-burnup fueled BWR samples.

During the post-test sample handling, the ICL#3 sample was broken three times. Cross-sectional SEM examinations were conducted for fractographic analysis at locations A and C of Fig. 9. Figure 14 shows typical fractographs of the oxide, the alpha phase, and the prior-beta-phase layers for the sample at location A. The failure region appears to be nearly brittle even in the prior-beta-phase area. No significant differences are observed between locations A and C.

Secondary Hydriding

Hydrogen is released during inner-surface oxidation within the balloon region, particularly near the burst region. Because of the resistance to flow through the small burst opening, a relatively high fraction of this hydrogen remains within the sample and migrates up and down the sample toward the burst neck-and-beyond regions. For the unirradiated samples, there is little resistance to this migration, and the bare cladding inner surface absorbs a large amount of hydrogen (see Fig. 4). Qualitatively, the same behavior would be expected for fresh and low-burnup fuel cladding. For high-burnup fuel, the axial extent of hydrogen that could come in contact with the cladding would be limited by the presence of the fuel, and

the local hydrogen absorption would be limited by the fuel-cladding bond layer. This layer has been shown to not be protective with regard to steam oxidation within the ballooned region. It is of great interest to determine whether or not the layer is protective with respect to hydrogen diffusion into the cladding. Hydrogen and oxygen concentrations were measured for ICL#2 and ICL#3 samples sectioned from different axial positions below and above the burst center. The raw data give oxygen and hydrogen concentrations. The hydrogen pickup and ECR can be determined by applying Eqs. 1 and 2 given in reference 3, the results of which are shown in Fig. 15. These results are compared to the peak hydrogen-content locations and values for OCL#11. This shows a significant difference in the post-LOCA behavior between the axial distribution of hydrogen in high-burnup cladding vs. nonirradiated cladding. The peaks of the hydrogen pickup in the high-burnup specimens are shifted toward the burst center, compared with the unirradiated samples. However, the maximum hydrogen pickups are nearly at the same level for both high burnup (≈3000 wppm) and unirradiated (3500 – 4000 wppm) specimens. More data are to be provided to map out the axial distribution of hydrogen pickup in high-burnup cladding subjected to the LOCA transient.

Effects of Hydrogen on Post-quench-ductility for Prehydrided 15x15 Zry-4

While extensive literature data are available for unirradiated Zry-4, relatively little data have been published for high-burnup PWR samples, which have a higher hydrogen content than BWR during normal operation in the reactor. The high-temperature steam oxidation tests and PQD tests with prehydrided Zry-4 provide some guidance for planning high-burnup PWR LOCA integral tests. In this program, all non-irradiated samples (as-received 15x15 Zry-4 and prehydrided 15x15 Zry-4) are oxidized at the same heatup rates, hold times, and cooling rates (slowly cooled to 800˚C and water-quenched). The 25-mm-long samples are exposed to two-sided steam oxidation prior to cooling. Also, the samples are compressed in the same Instron machine, and the load-displacement data are analyzed by a common method to determine ductility.

The 15x15 Zry-4 materials provided by Framatome ANP have an outer diameter of 10.75 mm and a wall thickness of 0.76 mm. Following steam oxidation and quench, 8-mm rings are cut from the 25-mm-long samples. Ring compression tests are performed at a cross-head displacement rate of 2 mm/min and room temperature, 100°C, and 135°C. The load-displacement curves are analyzed by the traditional offset-displacement method. The offset displacement, which is a measure of permanent displacement, is

normalized to the outer diameter (10.75 mm) to give a nominal plastic hoop strain. Samples that exhibit offset strains ≥3% are considered to be ductile. However, for samples with <3% offset strain, another method is used to better determine permanent deformation and ductility. For this second method, the sample is unloaded after the first significant load drop, indicating through-wall failure along the length of the sample. The post-test diameter along the loading direction is measured directly and compared to the pre-test diameter to give a direct measure of permanent strain. For these low-offset-strain samples, the permanent diameter change in the loading direction provides a direct measure of ductility. Rings that exhibit ≥1% permanent diameter change are considered to be ductile.

Oxidation and quench have been completed for as-received and prehydrided Zry-4 samples oxidized at 1204˚C. Weight gains were recorded for each sample, normalized to the oxidation surface area, and compared to CP predictions for weight gain (in mg/cm^2). For prehydrided samples hydrogen-content analyses have been performed before and after the steam oxidation tests. This characterization is performed to allow correlation between the ductility observed in the ring compression test and the microstructure (e.g., prior-beta-layer thickness, extent of alpha incursions into this layer, and the hydrogen content).

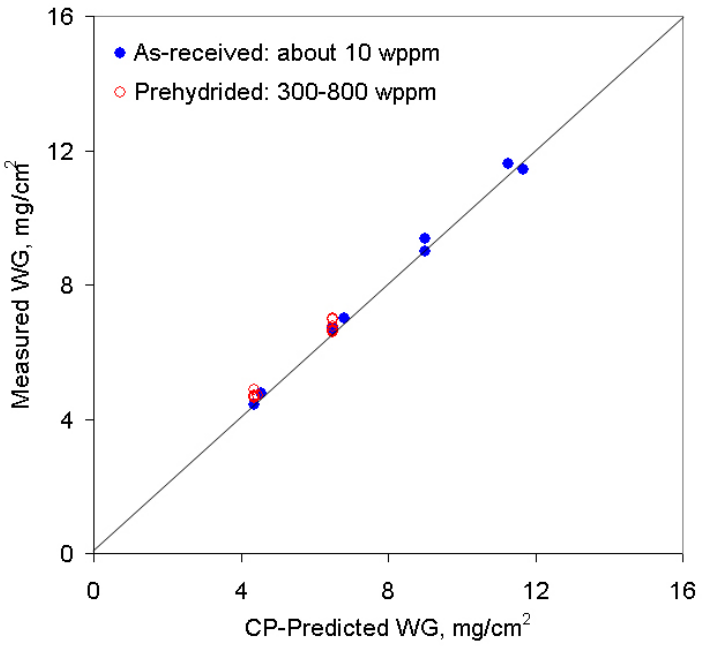

Fig. 16. Measured vs. predicted weight gain comparison of as-received and pre-hydrided samples for 15x15 Zry-4 after steam oxidation at ≈1204˚C.

Weight Gain Kinetics

The weight gain data for both as-received and prehydrided 15x15 Zry-4, oxidized at 1204˚C, were in excellent agreement with the CP-predicted weight gain values (see Fig. 16). At the longest test time, measured values were 11.45 mg/cm^2, as compared to the predicted value of 11.67 mg/cm^2. Using the measured wall thickness for each alloy, these weight-gain values convert to the "measured" ECR values of 13.2% in our tests. No significant hydrogen influence was found on the oxidation kinetics.

Post-quench-ductility Results

The load-displacement curves from the ring compression tests were analyzed by the offset method. Tests were stopped very shortly after the first significant load drop (≈30–50%), which indicated a through-wall crack along the length of the ring. The offset displacement prior to the first through-wall crack is determined mathematically by unloading the specimen at the elastic loading stiffness. Normalizing this offset displacement to the as-fabricated outer diameter gives an offset strain.

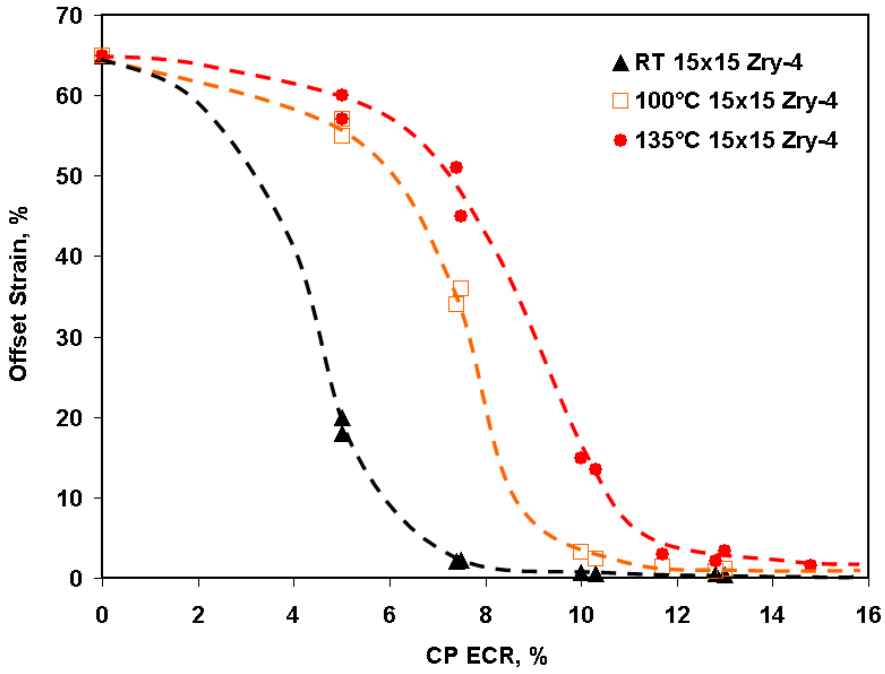

Fig. 17. Offset strain vs. CP ECR for as-received 15x15 Zry-4 oxidized at 1204°C (H < 25 wppm)

To evaluate the temperature influence on PQD, 25-mm-long samples were oxidized at 1204°C up to 13% ECR. Each sample was then cut into three 8-mm-long rings and tested at room temperature (RT), 100°C, and 135°C. It was found that the threshold of PQD shifts toward higher ECR values as the test temperature increases. For oxidized, as-received 15x15 Zry-4 samples (H < 25 wppm), embrittlement occurred at 8-9% ECR at RT; 11-12% ECR at 100°C; and 13-14% ECR at 135°C. Figure 17 shows the offset strain vs. ECR for as-received 15x15 Zry-4 oxidized at 1204°C.

It is well known that the post-LOCA test samples can be very brittle due to hydriding effects (pre-test H content and the H pickup during the steam oxidation). The pre-test hydrogen content during normal operation in reactors for high-burnup PWR samples is quite high (400-800 wppm), compared to high-burnup BWR samples. Thus, steam oxidation tests with prehydrided 15x15 Zry-4 were performed at 1204°C, followed by the ring compression tests, to study the effects of hydrogen on post-quench ductility. The hydrogen charging was performed at 400˚C in the flowing mixture gas 4% H_2-Ar, and the range of H-charging was carefully chosen to be close to the pre-test H content of the high-burnup PWR samples. Hydrogen analyses were conducted with the LECO hydrogen determinator on pre- and post-test samples.

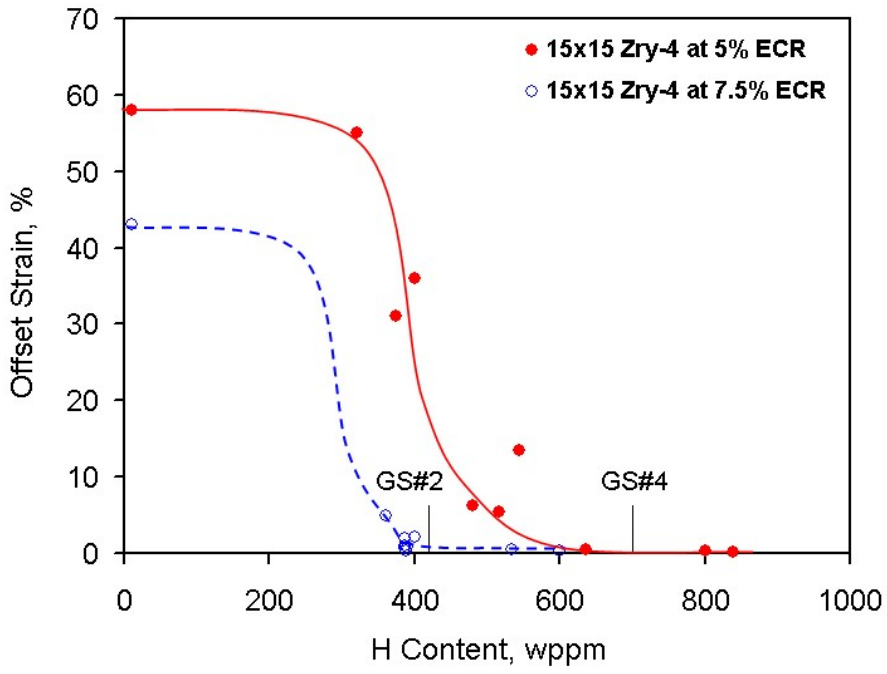

Fig. 18 Effects of hydrogen on post-quench ductility at 135°C for prehydrided 15x15 Zry-4 oxidized at 1204°C.

For samples oxidized at 1204˚C for 5% CP-ECR, the samples remained ductile until the hydrogen content increased > 550 wppm. For the 7.5% CP-ECR samples, the samples became brittle when the hydrogen content reached 400 wppm. The plot in Fig. 18 shows the effects of hydrogen on PQD at 135°C for prehydrided 15x15 Zry-4 oxidized at 1204°C.

Conclusions and Future Work

LOCA integral test results are reported for high-burnup BWR fuel specimens. These results are compared to baseline data for nonirradiated Zry-2 cladding specimens filled with zirconia pellets and exposed to the same tests. Four LOCA integral tests have been conducted with specimens from Limerick BWR fuel rods at 56 GWd/MTU, among which the ICL#4 specimen was exposed to the full LOCA sequence by heating in steam at 5˚C/s to 1204˚C, holding for 5 minutes at 1204˚C (20% CP-ECR), slow-cooling at 3˚C/s to 800˚C, and bottom-flooding to quench the cladding from 800 to 100˚C. The specimens were internally pressurized with helium to a gauge pressure of ≈8.3 MPa at 300˚C. During heating in steam at 5˚C/s, the internal pressure rose to ≤9 MPa prior to burst at ≈750˚C.

Nondestructive examinations included photography and profilometry for all four specimens and post-test gamma scanning for the ICL#3 and #4 specimens. Destructive examinations were performed on ICL#2 and #3 specimens to determine oxide layer thickness, fuel morphology, and axial profiles of hydrogen and oxygen concentration. Based on measurements of cladding outer- and inner-surface oxide thickness at several axial locations, it appears that the presence of ≈10 μm of corrosion does not inhibit or slow down outer-surface oxidation and the presence of a fuel and fuel-cladding bond does not retard inner-surface steam oxidation. Oxide-layer thickness and oxygen-content results indicate two-sided oxidation in the ballooned-and-burst region of both high-burnup and nonirradiated specimens. With regard to steam oxidation, high-burnup Zry-2 behaved very similarly to nonirradiated Zry-2 during the LOCA transient. The major post-LOCA difference observed between high-burnup fuel cladding and nonirradiated cladding was the degree of secondary hydriding in the balloon neck region. For nonirradiated specimens, the hydrogen pickup was low in the burst region and very high (≈3900 wppm) at 70-90 mm above and below the burst mid-plane. For high-burnup fuel cladding, the hydrogen peak (≈3000 wppm) was toward the burst mid-plane. Because of the large secondary hydriding from the cladding inner surface, significant degradation of PQD is expected for the ICL#4 ballooned region, even at 100-135˚C.

In the uniform burnup region (within grid spans 2-5), the high-burnup PWR cladding for the next set of LOCA tests differs from BWR cladding in terms of corrosion layer thickness (≈40 to 100 μm) and hydrogen content (≈400 to 800 wppm). For test planning purposes, the separate effects of hydrogen on diametral-compression PQD have been investigated with prehydrided, nonirradiated 15x15 Zry-4 cladding rings after oxidation at 1204˚C and quench. For as-received (≈10 wppm H) cladding that was oxidized at 1204˚C, the ductile-to-brittle-transition CP-ECR was 8-9% at room temperature, 11-12% at 100˚C, and 13-14% at 135˚C. In contrast, cladding with 400-to-800 wppm hydrogen exhibited significant embrittlement, even after moderate oxidation at 1204˚C. Samples prehydrided to 400-800 wppm and oxidized at 1204˚C to 8% CP-ECR exhibited no ductility. With anticipated secondary hydrogen uptake from the cladding inner surface, the embrittlement ECR in the balloon region is expected to be <<17% for high-burnup PWR specimens subjected to LOCA integral tests at 1204˚C, even if the ECR is determined by the sum of the corrosion layer and the BJ-calculated transient ECR. The baseline data from prehydrided cladding are being used to plan the PWR hold times at 1204˚C such that the embrittlement ECR can be determined effectively in the ballooned and non-ballooned regions of the PWR specimens from LOCA integral tests.

References

1. Y. Yan, R. V. Strain, T. S. Bray, and M. C. Billone, "High Temperature Oxidation of Irradiated Limerick BWR Cladding," Proceedings of the Nuclear Safety Research Conference (NSRC-2001), Washington, DC, October 22-24, 2001, NUREG/CP-0176 (2002) 353-372.

2. Y. Yan, R. V. Strain, and M. C. Billone, "LOCA Research Results for High-Burnup BWR Fuel," Proc. Nuclear Safety Research Conference (NSRC-2002), Washington, DC, October 28-30, 2002, NUREG/CP-0180 (2003) 127-155.

3. Y. Yan, T. Burtseva, and M. C. Billone, "LOCA Results for Advanced-alloy and High-burnup Zircaloy Cladding," Proc. Nuclear Safety Research Conference (NSRC-2003), Washington, DC, October 25-27

4. G. Hache and H. M. Chung, "The History of LOCA Embrittlement Criteria," Proc. 28th Water Reactor Safety Meeting, Bethesda, MD, October 23-25, 2000, NUREG/CP-0172 (2001) 205-237